RSC Mechanochemistry

ROYAL SOCIETY OF CHEMISTRY

PAPER

View Article Online
View Journal | View Issue

Cite this: *RSC Mechanochem.*, 2025, **2**, 763

Mechanochromic polymer particles crosslinked by a radical-type mechanochromophore†

Kengo Ogasawara,[a] Daisuke Kuromiya,[a] Takuma Watabe,[a] Akira Takahashi,[a] Daisuke Aoki[a] and Hideyuki Otsuka[*ab]

Received 24th May 2025
Accepted 14th July 2025

DOI: 10.1039/d5mr00071h

rsc.li/RSCMechanochem

The mechanochromic properties of polymer particles crosslinked by difluorenylsuccinonitrile (DFSN), a radical-type mechanochromophore, are reported in relation to particle size and glass transition temperature. DFSN-crosslinked nanoparticles and microparticles were prepared *via* emulsion polymerization and suspension polymerization of vinyl monomers, respectively, using a DFSN-containing crosslinker. Mechanical grinding of the prepared white particles induced a pink coloration, originating from cyanofluorenyl (CF) radicals generated by the mechanically induced homolysis of DFSN units within the particles. The mechanochemical response of the particles was evaluated using scanning electron microscopy and electron paramagnetic resonance spectroscopy, revealing that microparticles exhibited a stronger response than nanoparticles due to the differences in pulverization behavior. The mechanochemical response also showed a strong correlation with the glass transition temperatures of the particles, highlighting the importance of polymer chain mobility in the mechanochromic properties of the developed polymer particles.

Introduction

Stimuli-responsive polymers, which exhibit new properties and behaviors in response to physical or chemical stimuli such as light,[1] magnetic fields,[2] and pH changes,[3] have recently attracted considerable attention in fields such as medicine, biology, and materials science. In particular, mechanochromic polymers, which display color changes and fluorescence emission in response to mechanical stimuli, have been increasingly studied due to their potential applications in detecting stress and damage in materials.[4–6] These polymers are typically designed by incorporating functional molecules known as mechanochromophores or mechanofluorophores, such as spiropyrans,[7] naphthopyrans,[8] dioxetanes,[9] rhodamines,[10] Diels–Alder adducts,[11] and others.[12–15] Upon exposure to mechanical stimuli, these molecules undergo structural transformations resulting in changes in color and/or fluorescent properties.

Polymer particles have found widespread applications across various industrial fields, such as cosmetics, pigments, paints, and modifiers.[16] In the field of polymer materials, such particles are referred to as fillers and are used to enhance material properties[17–21] in a similar manner to silica particles[22,23] and carbon black.[24,25] Meanwhile, mechanochromic polymer particles have recently emerged as a novel class of functional polymer particles. Göstl and co-workers developed epoxy resin composites incorporating poly(hexyl acrylate) particles crosslinked by a maleimide–anthracene adduct, which undergoes a retro-Diels–Alder reaction in response to mechanical damage, resulting in fluorescence emission and visualization of particle–crack interactions.[26] Jang *et al.* reported polydimethylsiloxane particles crosslinked with a spiropyran mechanochromophore, which were introduced into various polymer matrices to visualize spatial stress distribution.[27] Thus, mechanochromic polymer particles can serve as additives to not only enhance the toughness of base materials but also visualize damage sustained by the materials. However, little is known about the relationship between particle structure and mechanoresponsiveness due to the challenges associated with quantitative analysis.

In this context, radical-type mechanochromophores, which undergo homolysis under mechanical stimuli to generate semistable, colored radicals, are advantageous for quantitatively evaluating mechanical damage due to their ability to be quantified using electron paramagnetic resonance (EPR) spectroscopy. In the past decade, our group has demonstrated a wide variety of polymers featuring radical-type mechanochromophores,[28,29] including star polymers[30] and dendrimers,[31] to reveal aspects of structure–reactivity relationships in bulk polymer mechanochemistry. Recently, we developed a difluorenylsuccinonitrile (DFSN) mechanochromophore, which generates pink-colored cyanofluorenyl (CF) radicals in response to mechanical stimuli (Fig. 1a).[32–42] CF radicals are relatively

[a]*Department of Chemical Science and Engineering, Institute of Science Tokyo, 2-12-1 Ookayama, Meguro-ku, Tokyo 152-8550, Japan. E-mail: otsuka@mac.titech.ac.jp*
[b]*Research Center for Autonomous Systems Materialogy (ASMat), Institute of Integrated Research, Institute of Science Tokyo, Japan*

† Electronic supplementary information (ESI) available. See DOI: https://doi.org/10.1039/d5mr00071h

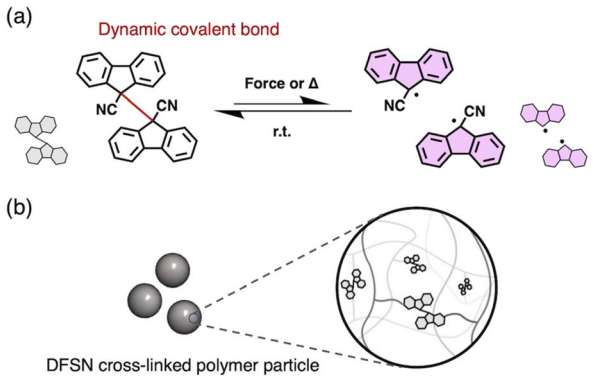

Fig. 1 (a) Equilibrium between DFSN and its radical species. (b) Conceptual illustration of DFSN crosslinked polymer particles.

stable against oxygen, while DFSN exists exclusively in a dimer state at temperatures below 40 °C, thereby not interfering with radical polymerization at lower temperatures. In this study, we developed DFSN crosslinked polymer particles and investigated the effect of particle architectures on their mechanochromic reactivity (Fig. 1b).

Experimental

Materials

All reagents and solvents were purchased from Sigma-Aldrich, FUJIFILM Wako Pure Chemical Corporation, Tokyo Chemical Industry, or Kanto Chemical, and used as received unless otherwise noted. Methyl methacrylate (MMA), ethyl methacrylate (EMA), and propyl methacrylate (PMA) were passed through a basic alumina column (Merck KGaA) to remove the stabilizer before use. The DFSN crosslinker with two methacryloyl groups (**DFSN-dimethacrylate**) were synthesized according to the previously published method.[33]

Measurements

^{1}H NMR spectroscopic measurements were carried out using a 500 MHz Bruker spectrometer with tetramethylsilane (TMS) as an internal standard in chloroform-*d* ($CDCl_3$) or dimethyl sulfoxide-d_6 (DMSO-d_6). FT-IR spectra were recorded on a JASCO FT/IR-4100 with a KBr plate. Size exclusion chromatography (SEC) measurements were carried out at 40 °C on a TOSOH HLC-8320 SEC system equipped with a guard column (TOSOH TSK guard column SuperH-L), three columns (TOSOH TSK gel SuperH 6000, 4000, and 2500) and a differential refractive index detector. Tetrahydrofuran (THF) was used as the eluent at a flow rate of 0.6 mL min^{-1}. Polystyrene standards (M_n = 4430–3242000; M_w/M_n = 1.03–1.08) were used to calibrate the SEC system. Differential scanning calorimetry (DSC) was carried out using a Shimadzu DSC-60A differential scanning calorimeter. Samples were measured at a heating rate of 10 °C min^{-1} between 0 °C and 160 °C with a time interval of 2 min under N_2 flow. Scanning electron micrographs were obtained using scanning electron microscope (SEM; KEYENCE, VE9800, Japan). A drop of aqueous dispersion (*ca.* 1 mg mL^{-1}, 30–50 μL) was placed onto a carbon tape (5 × 5 mm) and then evaporated to dryness in a dust-free box at room temperature. The sample was then sputter-coated with Pd/Pt under vacuum using an ion sputter (Hitachi, Ltd, E-1010, Japan). Particle size distribution measurements were carried out using a laser diffraction particle size analyzer (Shimadzu, SALD-2300 WingSALD II: Version 3.4.6, Japan). A dilute aqueous solution of the particle was scanned 128 times with a time interval of 2 seconds under continuous stirring at room temperature.

Synthesis of DFSN crosslinked nanoparticles (DFSN-NPs)

MMA3/EMA7-NP. A solution of *N*,*N*,*N*′,*N*′-tetramethylethylenediamine (TEMED) (2.32 mg, 2.00 μmol) in water (10 mL) was degassed in a test tube (internal diameter: 30 mm, length: 130 mm) by bubbling with N_2 for 10 minutes. A solution of MMA (0.300 g, 3.00 mmol), EMA (0.799 g, 7.00 mmol), and **DFSN-dimethacrylate** (0.0751 g, 0.100 mmol), which had been degassed by at least three freeze-pump-thaw cycles, was transferred into the reactor. A 10 mM potassium persulfate (KPS) aqueous solution (2.0 mL) was added to the reactor. The solution was then stirred at 35 °C with an oval-type magnetic stirrer (Φ = 20 mm) at 700 rpm for 22 hours. The reaction was quenched by exposure to air and dilution with water, and the resulting emulsion was centrifuged for 10 min (9500 rpm, 0 °C). The supernatant was then decanted, followed by rinsing the remaining precipitate with water (2 times) and methanol (2 times). The precipitate was dried under vacuum at room temperature for 24 hours to afford **MMA3/EMA7-NP** as a colorless powder (0.542 g, 46% yield).

EMA-NP. The sample was synthesized in a similar manner to **MMA3/EMA7-NP** using EMA (1.14 g, 10.0 mmol), **DFSN-dimethacrylate** (0.0751 g, 0.100 mmol), KPS (5.41 mg, 2.00 μmol), TEMED (2.32 mg, 2.00 μmol), and water (10 mL). **EMA-NP** was obtained as a colorless powder (0.608 g, 50% yield).

EMA5/PMA5-NP. The sample was synthesized in a similar manner to **MMA3/EMA7-NP** using EMA (0.571 g, 5.00 mmol), PMA (0.641 g, 5.00 mmol), **DFSN-dimethacrylate** (0.0751 g, 0.100 mmol), KPS (5.41 mg, 2.00 μmol), TEMED (2.32 mg, 2.00 μmol), and water (10 mL). **EMA5/PMA5-NP** was obtained as a colorless powder (0.597 g, 46% yield).

MMA-NPs with different particle size (663-NP, 754-NP, and 1223-NP). The samples were synthesized in a similar manner to **MMA3/EMA7-NP** using MMA (1.00 g, 10.0 mmol), **DFSN-dimethacrylate** (0.0751 g, 0.100 mmol), KPS (5.41 mg, 2.00 μmol), TEMED (2.32 mg, 2.00 μmol), and a water/methanol mixed solvent (water/methanol = 7/3–5/5, v/v, 10 mL in total). **MMA-NPs** with different particle sizes were obtained as colorless powders (0.892 g, 83% yield for **663-NP**, 1.04 g, 90% yield for **754-NP**, and 0.863 g, 80% yield for **1223-NP**).

Synthesis of DFSN crosslinked microparticles (DFSN-MPs)

MMA-MP. A solution of MMA (0.936 g, 9.35 mmol) and **DFSN-dimethacrylate** (0.0702 g, 0.0935 mmol) was degassed by three freeze-pump-thaw cycles. 2,2′-Azobis(4-methoxy-2,4-dimethylvaleronitrile) (V-70) (34.6 mg, 0.112 mmol) was added, and the solution was then degassed by freeze-pump-

thaw cycles. After 20 minutes of stirring at 25 °C, the solution was transferred *via* a syringe into a test tube (internal diameter: 35 mm, length: 135 mm) containing 20 mL of 0.3 wt% PVA aqueous solution, which had been degassed by bubbling with N_2 for 20 minutes, followed by stirring at 35 °C with an oval-type magnetic stirrer (ϕ = 25 mm) at 700 rpm for 22 hours. The reaction was quenched by exposure to air and dilution with water, and the resulting suspension was centrifuged for 10 min (9500 rpm, 0 °C). The supernatant was decanted, and the remaining precipitate was then washed with water (2 times) and methanol (2 times). The remaining precipitate was dried under vacuum at room temperature for 24 hours to afford **MMA-MP** as a colorless powder (0.563 g, 56% yield).

EMA-MP. The sample was synthesized in a similar manner to **MMA-MP** using EMA (1.07 g, 9.35 mmol), **DFSN-dimethacrylate** (0.0702 g, 0.0935 mmol), V-70 (34.6 mg, 0.112 mmol), and 0.3 wt% PVA solution (20 mL). **EMA-MP** was obtained as a colorless powder (0.559 g, 49% yield).

EMA5/PMA5-MP. The sample was synthesized in a similar manner to **MMA-MP** using EMA (0.534 g, 4.68 mmol), PMA (0.599 g, 4.68 mmol), **DFSN-dimethacrylate** (0.0702 g, 0.0935 mmol), V-70 (34.6 mg, 0.112 mmol), and 0.3 wt% PVA solution (20 mL). **EMA5/PMA5-MP** was obtained as a colorless powder (0.662 g, 55% yield).

PMA-MP. The sample was synthesized in a similar manner to **MMA-MP** using PMA (1.20 g, 9.35 mmol), **DFSN-dimethacrylate** (0.0702 g, 0.0935 mmol), V-70 (34.6 mg, 0.112 mmol), and 0.3 wt% PVA solution (20 mL). **PMA-MP** was obtained as a colorless powder (0.861 g, 68% yield).

Grinding tests and EPR study in solid states

Grinding tests were performed on a Retsch Mixer Mill MM 400. The mechanical energy was controlled by vibrational frequency and grinding time. A sample (50 mg) and a stainless steel ball (d = 5 mm) were placed in the grinding jar and ball-milled for 10 min at 30 Hz. The ground sample was transferred into a glass capillary (d = 5 mm), and the capillary was sealed after being degassed. EPR measurements were carried out on a JEOL JES-X320 X-band EPR spectrometer equipped with a JEOL DVT temperature controller. The spectra of the ground samples were measured using a microwave power of 0.1 mW and field modulation of 7.5 mT with a time constant of 0.03 s and a sweep rate of 0.125 mT s^{-1} at room temperature. The concentration of the radicals formed from the cleavage of DFSN was determined by comparing the area of the integral spectrum with a 0.02 mM solution of 4-hydroxy-2,2,6,6-tetramethylpiperidin-1-oxyl (TEMPOL) in benzene under the same experimental conditions. The Mn^{2+} signal was used as an auxiliary standard. The g value was calculated according to the following equation: $g = h\nu/\beta H$, where h is the Planck constant, ν is the microwave frequency, β is the Bohr magneton, and H is the magnetic field.

Decrosslinking experiments

Typically, **DFSN-MMA3/EMA7-NP** (20.0 mg, theoretically 1.70 μmol of DFSN skeleton) was immersed in 2.00 mL of a DFSN-model solution in anisole (20.0 mg, 52.6 μmol), which was pre-degassed by bubbling with N_2 for 20 minutes. The solution was heated at 110 °C under a N_2 atmosphere for 2 days. The resulting solution was filtered, and the obtained filtrate was purified by precipitation into cold methanol (0 °C). The precipitates were collected by filtration and dried under reduced pressure to afford a white powder (7.8 mg, 39% yield).

Results and discussion

DFSN crosslinked nanoparticles (**DFSN-NP**s) were prepared by surfactant-free emulsion polymerization using KPS and TEMED, which form a redox initiator system that allows the polymerization at mild temperatures to suppress the thermal dissociation of DFSN. Furthermore, it has also been reported that sulfonic acid groups remain on the particle surface in this system, stabilizing the dispersion through electrostatic repulsion even in the absence of an emulsifier.[43] The feed ratio of crosslinker to monomer was set at 1 mol% for all samples. To evaluate the size effect on the mechanochromic property, **DFSN-NP**s of PMMA with different diameters were prepared in a water/methanol mixture with varying ratios (Scheme 1 (left)).[44] The formation of the particles was confirmed by scanning electron microscopy (SEM) (Fig. 2a (top)), and the image analysis revealed the formation of uniform nanoparticles with mean diameters of 663, 754, and 1223 nm, referred to as **663-NP**, **754-NP**, and **1223-NP**, respectively. We also prepared **DFSN-NP**s with different glass transition temperatures (T_g) using three methacrylate monomers (MMA, EMA, and PMA) to evaluate the effect of chain mobility on the mechanochromic property. The monomer feed ratios were MMA/EMA = 3/7, EMA only, and EMA/PMA = 5/5, resulting in the corresponding **DFSN-NP**s (**MMA3/EMA7-NP**, **EMA-NP**, and **EMA5/PMA5-NP**) with uniform sizes. DSC measurements revealed T_g values of 73 °C for **MMA3/EMA7-NP**, 65 °C for **EMA-NP**, and 51 °C for **EMA5/PMA5-NP**, respectively (Fig. S3†). While MMA-based **DFSN-NP**s were obtained in good yields (80–90%), the other **DFSN-NP**s with

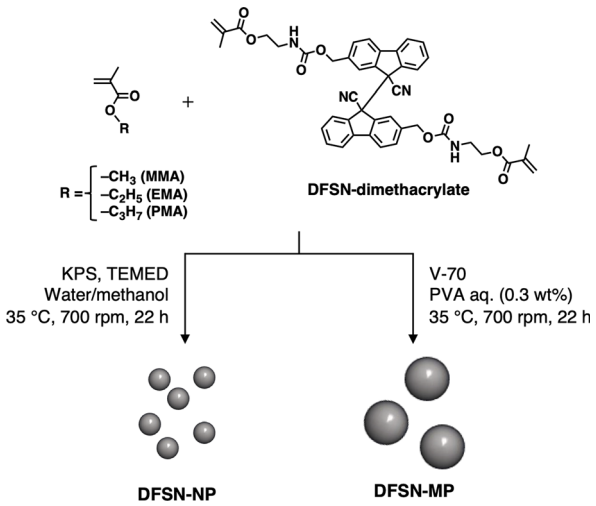

Scheme 1 Synthesis of DFSN-NPs by surfactant-free emulsion polymerization and DFSN-MPs by suspension polymerization.

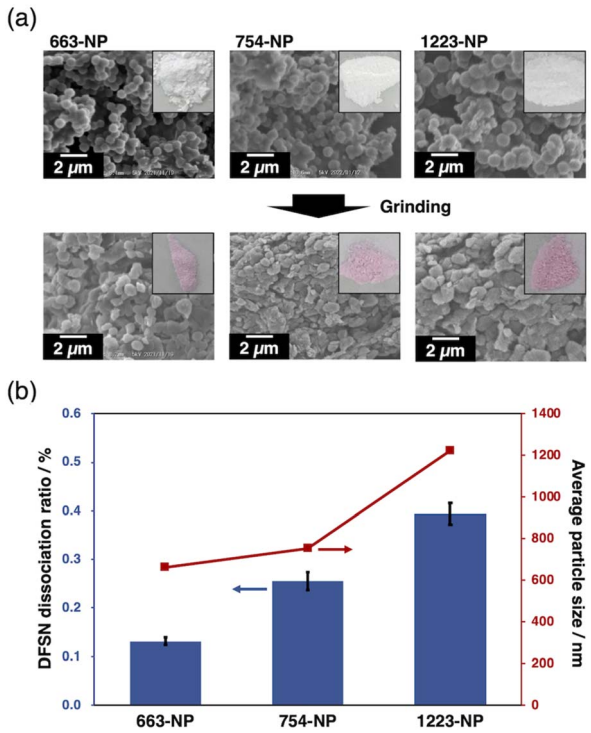

Fig. 2 (a) Photographs and SEM images of DFSN-NPs with different particle sizes before and after grinding. (b) Dissociation ratios of DFSN skeletons in ground DFSN-NPs with different original particle sizes.

different compositions resulted in relatively low yields (approximately 50%) due to polymer adhesion to the reaction vessel. This adhesion is attributed to the agglomeration of polymers, caused by polymerization at low temperatures.[43] Since this phenomenon could lead to a discrepancy between the feed ratio and the polymer composition, further optimization of the nanoparticle synthesis method will be necessary for **MMA3/EMA7-NP**, **EMA-NP**, and **EMA5/PMA5-NP**. The detailed synthetic results are summerized in Table S1.†

To evaluate the mechanoresponsiveness of **DFSN-NP**s, grinding tests were performed using a ball mill (30 Hz, 10 min) at room temperature. The PMMA-based **DFSN-NP**s with different particle sizes showed color changes to pale pink (Fig. 2a (inset)), suggesting the formation of CF radicals that absorb visible light due to the dissociation of the DFSN unit. EPR measurements for the ground samples were conducted to confirm the cleavage of the DFSN. The measurements displayed spectra with g values of 2.003 (Fig. S4†), which can be attributed to DFSN-derived CF radicals. The coloration after grinding was more vibrant as the particle size increased, and this correlation was supported by the EPR spectra; the DFSN dissociation ratios were calculated to be 0.13% for **663-NP**, 0.26% for **754-NP**, and 0.39% for **1223-NP** (Fig. 2b). SEM observations revealed that the particle shape became flattened and partially fused after ball-milling (Fig. 2a (bottom)), suggesting that the applied energy was consumed by deformation, collisions, and agglomeration of the nanoparticles. Importantly, the shape change was more significant for larger nanoparticles. These results clearly indicate that the mechanical stimuli during ball milling are transmitted more efficiently in larger particles. Such a size effect has also been reported by Fu and Wang.[45]

On the other hand, **MMA3/EMA7-NP**, **EMA-NP**, and **EMA5/PMA5-NP** hardly changed color upon grinding (Fig. 3a (inset)). The SEM images of the ground samples showed that the nanoparticles were deformed in a similar manner to the PMMA-based nanoparticles due to grinding, confirming the application of mechanical force to the nanoparticles. In fact, the EPR spectra of the ground nanoparticles showed spectra consistent with carbon-centered radicals ($g = 2.003$) (Fig. S5†), indicating the formation of DFSN-derived CF radicals. However, the dissociation ratios of the DFSN skeletons were calculated to be 5.1×10^{-3}% (**MMA3/EMA7-NP**), 2.4×10^{-3}% (**EMA-NP**), and 9.5×10^{-4}% (**EMA5/PMA5-NP**), respectively (Fig. 2b), which are approximately two orders of magnitude smaller compared to the PMMA-based nanoparticles. Additionally, the dissociation ratio was positively correlated with the T_g of the polymers. These results suggest the importance of the rigidity of polymer chains for mechanochromism, presumably because rigid polymer chains are advantageous for suppressing the recombination of CF radicals due to the limited molecular mobility. Also, to examine whether the order of the mechanical response is determined not by T_g but by the amount of DFSN introduced into the nanoparticles, we attempted to evaluate the DFSN content in **MMA3/EMA7-NP**, **EMA-NP**, and **EMA5/PMA5-NP**, which showed low yields during synthesis, by decrosslinking

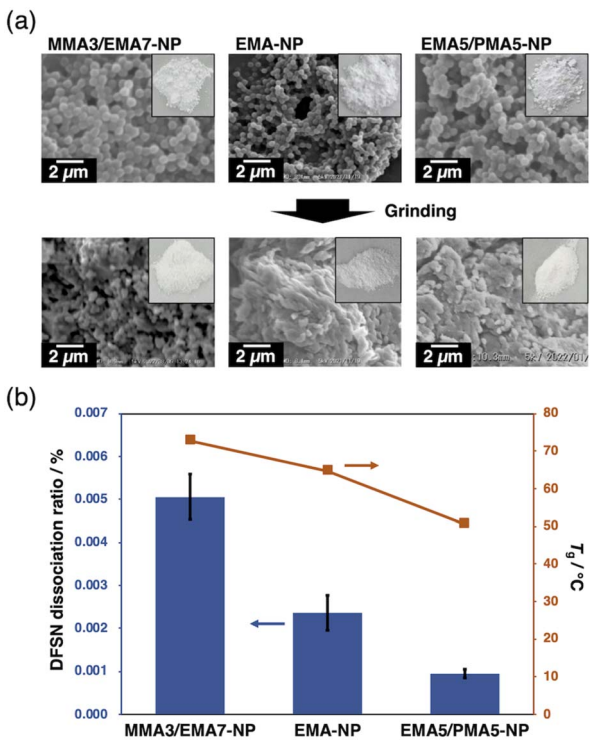

Fig. 3 (a) Photographs and SEM images of DFSN-NPs with different polymer compositions before and after grinding. (b) Dissociation ratios of DFSN skeletons in ground DFSN-NPs with different polymer compositions and T_g.

experiments. Each sample was reacted with 31–34 eq. of pristine DFSN molecule at 110 °C to induce decrosslinking *via* bond exchange reactions.[32] However, insoluble fractions remained after the reaction, and the yields of the soluble fractions were limited to 39% for **MMA3/EMA7-NP**, 73% for **EMA-NP**, and 61% for **EMA5/PMA5-NP**. ^{1}H NMR spectra of the soluble fractions displayed the peaks of DFSN moieties with comparable peak intensities (Fig. S7†), but they cannot be quantitatively compared due to the incomplete solubilization of the **NP**s. GPC measurements of the soluble fractions revealed a high M_n of 200 000–330 000 (Fig. S8†), suggesting the presence of a dense entanglement within the NPs that may hinder the exchange reaction and/or solubilization after decrosslinking.

To further expand the scope of mechanochromic polymer particles, DFSN-crosslinked microparticles (**DFSN-MP**s), which are approximately three orders of magnitude larger than **DFSN-NP**s, were next prepared by suspension polymerization using MMA, EMA, an EMA/PMA mixture (5/5), and PMA as the monomers and V-70 as the initiator (Scheme 1 (right)). The formation of the particles was confirmed by SEM in the same manner as **DFSN-NP**s, confirming the formation of uniform microparticles (Fig. 4a (top)). The T_g of the obtained **DFSN-MP**s was shown by DSC to be 123, 75, 67, and 48 °C for PMMA, PEMA, P(EMA-*co*-PMA), and PPMA-based microparticles, respectively (Fig. S3†).

The mechanoresponsiveness of **DFSN-MP**s was evaluated in the same manner as that of **DFSN-NP**s. Grinding tests of **DFSN-MP**s resulted in a pink coloration for all samples (Fig. 4a, inset). The SEM images of the ground samples showed pulverization of the particles (Fig. 4a), which presented a significantly different appearance compared to **DFSN-NP**s. The DFSN dissociation ratio of **MMA-MP**, estimated from EPR measurements (Fig. S6†), was 2.3%, which is 18 times larger than that of the PMMA-based nanoparticle with a diameter of 663 nm (**663-NP**). Such a large increase can be attributed to the much more vigorous pulverization behavior of the microparticles, as observed in the SEM, showing that the microparticles underwent significant stress during the grinding process. The dissociation ratios of the DFSN skeletons in **DFSN-MP**s were positively correlated with the T_g (Fig. 4b), similar to that of **DFSN-NP**s, again suggesting that the rigidity of the polymer chains contributes to the efficient dissociation of the DFSN skeletons. The pink color of the ground **DFSN-MP**s disappeared immediately upon adding good solvents like chloroform (Fig. S9†), which improves polymer chain mobility and promotes the recombination of the CF radicals.[32]

Fig. 5 shows the decay of the mechanically produced CF radicals over time, in which the amount of the radicals immediately after grinding was standardized to 1. The measurements showed a clear negative correlation between the decay rate and the T_g of the samples. Considering the recombination nature of the CF radicals, which is also indicated by the solvent addition experiment described above, the slow decay rate of the higher T_g samples is attributed to more restricted radical recombination due to limited chain mobility. Additionally, the initial fast decay of the radical amount for **PMA-MP** suggests that its low mechanical response (Fig. 4b) is attributed not only to the energy dissipation due to plastic deformation but also to the rapid recombination of CF radicals immediately after the mechanical dissociation of the DFSN unit. We also evaluated the decay rate of PMMA-based **663-NP** after grinding under the same conditions and compared the results with **MMA-MP**. The experiment resulted in a much faster decay for **663-NP** compared to **MMA-MP** (Fig. S10†). Considering that **DFSN-NP**s were only deformed and partially fused by ball mill whereas **DFSN-MP**s were pulverized, and that the radical recombination is under diffusion control, the diffusion region of the generated CF radicals during grinding may be narrower for **663-NP**, leading to faster CF radical recombination.

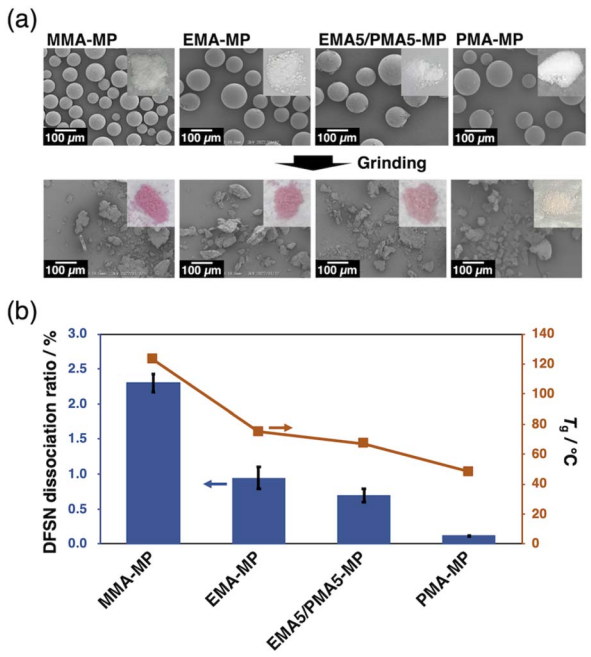

Fig. 4 (a) Photographs and SEM images of **DFSN-MP**s with different polymer compositions before and after grinding. (b) Dissociation ratios of DFSN skeletons in ground **DFSN-MP**s with different polymer compositions and T_g.

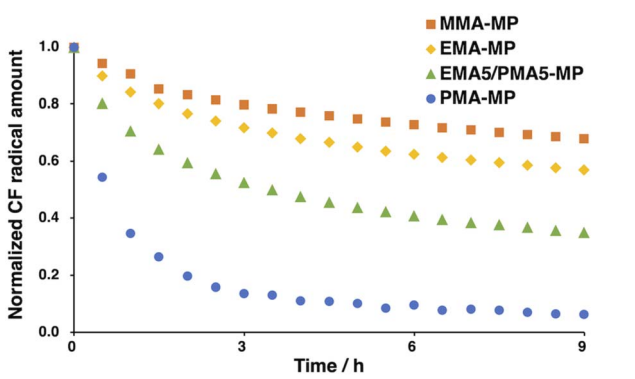

Fig. 5 Variation in the normalized dissociation ratio of DFSN skeletons in **DFSN-MP**s with different polymer compositions after grinding.

Conclusion

In summary, we evaluated the mechanoresponsiveness of polymer particles with DFSN skeletons at the crosslinking points of polymer chains. Several mechanochromic particles with different compositions and particle sizes were synthesized by emulsion polymerization for **DFSN-NP**s and by suspension polymerization for **DFSN-MP**s. Grinding tests and quantitative EPR measurements clarified that the large particle size and high T_g of the base polymer are important factors for efficient DFSN dissociation and the suppression of discoloration due to the recombination of CF radicals. These results provide beneficial insights into designing high-performance mechanochromic particles and help endow mechanochromic properties to various polymer materials through the use of mechanochromic particles as fillers. Meanwhile, the mechanochemical response of the mechanochromic particles may vary when they are actually incorporated in polymer matrices and exposed to different types of mechanical stimuli, and further investigation will be necessary to clarify the relationship with the results observed in this study.

Data availability

The data supporting this article have been included as part of the ESI.†

Conflicts of interest

There are no conflicts to declare.

Acknowledgements

This work was financially supported by JST CREST grant JPMJCR1991 from the Japan Science and Technology Agency (JST).

Notes and references

1 J. S. Katz and J. A. Burdick, *Macromol. Biosci.*, 2010, **10**, 339–348.
2 J. Thévenot, H. Oliveira, O. Sandre and S. Lecommandoux, *Chem. Soc. Rev.*, 2013, **42**, 7099–7116.
3 S. Dai, P. Ravi and K. C. Tam, *Soft Matter*, 2008, **4**, 435.
4 M. Stratigaki and R. Göstl, *ChemPlusChem*, 2020, **85**, 1095–1103.
5 Y. Chen, G. Mellot, D. van Luijk, C. Creton and R. P. Sijbesma, *Chem. Soc. Rev.*, 2021, **50**, 4100–4140.
6 W. Qiu, J. M. P. Scofield, P. A. Gurr and G. G. Qiao, *Macromol. Rapid Commun.*, 2022, **43**, 2100866.
7 D. A. Davis, A. Hamilton, J. Yang, L. D. Cremar, D. Van Gough, S. L. Potisek, M. T. Ong, P. V. Braun, T. J. Martínez, S. R. White, J. S. Moore and N. R. Sottos, *Nature*, 2009, **459**, 68–72.
8 M. J. Robb, T. A. Kim, A. J. Halmes, S. R. White, N. R. Sottos and J. S. Moore, *J. Am. Chem. Soc.*, 2016, **138**, 12328.
9 Y. Chen, A. J. H. Spiering, S. Karthikeyan, G. W. M. Peters, E. W. Meijer and R. P. Sijbesma, *Nat. Chem.*, 2012, **4**, 559–562.
10 Z. Wang, Z. Ma, Y. Wang, Z. Xu, Y. Luo, Y. Wei and X. Jia, *Adv. Mater.*, 2015, **27**, 6469–6474.
11 R. Göstl and R. P. Sijbesma, *Chem. Sci.*, 2016, **7**, 370–375.
12 Z. S. Kean, G. R. Gossweiler, T. B. Kouznetsova, G. B. Hewage and S. L. Craig, *Chem. Commun.*, 2015, **51**, 9157–9160.
13 H. Zhang, F. Gao, X. Cao, Y. Li, Y. Xu, W. Weng and R. Boulatov, *Angew. Chem., Int. Ed.*, 2016, **55**, 3040–3044.
14 M. Karman, E. Verde-Sesto, C. Weder and Y. C. Simon, *ACS Macro Lett.*, 2018, **7**, 1099–1104.
15 Y. Sagara, M. Karman, A. Seki, M. Pannipara, N. Tamaoki and C. Weder, *ACS Cent. Sci.*, 2019, **5**, 874–881.
16 J. H. Yeum, H. D. Ghim and Y. Deng, *Fibers Polym.*, 2005, **6**, 277–283.
17 A. G. Evans, Z. B. Ahmad, D. G. Gilbert and P. W. R. Beaumont, *Acta Metall.*, 1986, **34**, 79–87.
18 J. Wang, X. Zhang, L. Jiang and J. Qiao, *Prog. Polym. Sci.*, 2019, **98**, 101160.
19 S. Wu, *J. Appl. Polym. Sci.*, 1988, **35**, 549–561.
20 S. Wu, *Polym. Eng. Sci.*, 1990, **30**, 753–761.
21 Y. Yan, Y. Sun, J. Su, B. Li and P. Zhou, *Polymers*, 2023, **15**, 1375.
22 C. Su, X. Wang, L. Ding and Z. Wu, *Constr. Build. Mater.*, 2020, **262**, 120769.
23 H. R. Lee, M. I. Kim, H. R. Na, C. S. Lim and B. K. Seo, *Key Eng. Mater.*, 2017, **737**, 262–268.
24 X. Liang, M. Ito and K. Nakajima, *Polymers*, 2021, **13**, 3922.
25 B.-J. Lee and H.-M. Yoo, *Polymers*, 2024, **16**, 933.
26 M. Stratigaki, C. Baumann and R. Göstl, *Macromolecules*, 2022, **55**, 1060–1066.
27 H. G. Jang, J. Y. Jo, H. Park, Y. C. Jung, Y.-S. Choi, S. Jung, D. C. Lee and J. Kim, *Adv. Mater. Technol.*, 2023, **8**, 2200566.
28 T. Watabe and H. Otsuka, *Macromolecules*, 2024, **57**, 425–433.
29 T. Yamamoto, A. Takahashi and H. Otsuka, *Bull. Chem. Soc. Jpn.*, 2024, **97**, uoad004.
30 H. Oka, K. Imato, T. Sato, T. Ohishi, R. Goseki and H. Otsuka, *ACS Macro Lett.*, 2016, **5**, 1124–1127.
31 T. Watabe, D. Aoki and H. Otsuka, *Macromolecules*, 2021, **54**, 1725–1731.
32 H. Sakai, T. Sumi, D. Aoki, R. Goseki and H. Otsuka, *ACS Macro Lett.*, 2018, **7**, 1359–1363.
33 H. Sakai, D. Aoki, K. Seshimo, K. Mayumi, S. Nishitsuji, T. Kurose, H. Ito and H. Otsuka, *ACS Macro Lett.*, 2020, **9**, 1108–1113.
34 Y. Mao, T. Kubota, T. Kurose, A. Ishigami, K. Seshimo, D. Aoki, H. Otsuka and H. Ito, *Macromolecules*, 2020, **53**, 9313–9324.
35 K. Seshimo, H. Sakai, T. Watabe, D. Aoki, H. Sugita, K. Mikami, Y. Mao, A. Ishigami, S. Nishitsuji, T. Kurose, H. Ito and H. Otsuka, *Angew. Chem., Int. Ed.*, 2021, **60**, 8406–8409.
36 K. Yanada, D. Aoki and H. Otsuka, *Soft Matter*, 2022, **18**, 3218–3225.

37 Y. Mao, Y. Kubota, J. Gong, T. Kurose, A. Ishigami, K. Seshimo, T. Watabe, D. Aoki, H. Otsuka and H. Ito, *Macromolecules*, 2021, **54**, 8664–8674.
38 Y. Mao, Y. Kubota, R. Feng, J. Gong, A. Ishigami, Y. Kobayashi, T. Watabe, D. Aoki, H. Otsuka and H. Ito, *Macromolecules*, 2022, **55**, 3948–3957.
39 T. Watabe, D. Aoki and H. Otsuka, *Macromolecules*, 2022, **55**, 5795–5802.
40 T. Watabe and H. Otsuka, *Angew. Chem., Int. Ed.*, 2023, **62**, e202216469.
41 W. Khawdas, Y. Kubota, T. Yamamoto, H. Otsuka and H. Ito, *Macromolecules*, 2024, **57**, 7245–7252.
42 W. Khawdas, R. Iijima, K. Onuma, H. Otsuka and H. Ito, *Macromolecules*, 2025, **57**, 3537–3546.
43 T. Tanrisever, O. Okay and I. Ç. Sönmezoğlu, *J. Appl. Polym. Sci.*, 1996, **61**, 485–493.
44 S. E. Shim, K. Kim, S. Oh and S. Choe, *Macromol. Res.*, 2004, **12**, 240–245.
45 M. W. Fu and J. L. Wang, *Int. J. Mach. Tools Manuf.*, 2021, **167**, 103755.